

# Coupling LES, radiation and structure in gas turbine simulations

By J. Amaya<sup>†</sup>, E. Collado<sup>†</sup>, B. Cuenot<sup>†</sup> AND T. Poinsot<sup>‡</sup>

Multi-physics coupled simulations are performed to study the temperature field in a turbine blade placed in the high pressure distributor of a helicopter engine. Large Eddy Simulation (LES) is used to calculate the unsteady reacting flow in the chamber and is coupled to the simulation of radiation and heat conduction in the high pressure stator (HPS). This implies the use of three different solvers, running simultaneously on a parallel machine with an optimized processor distribution. Results are shown for the LES alone, for the LES coupled to heat conduction only and for the three coupled codes. The present demonstrate that the temperature field in the fluid and in the HPS are sensitive to both heat conduction and radiation, and that these two phenomena must be included to accurately predict the HPS temperature.

---

## 1. Introduction

Large Eddy Simulation (LES) is a powerful tool for the study of realistic combustors (Mahesh *et al.* 2006; Moin & Apte 2006; Schmitt *et al.* 2007; Lacaze *et al.* 2009) but its applicability remains limited if it is not coupled with other physical phenomena. Radiation and heat transfer through the walls of a combustion chamber are two obvious examples of mechanisms that play an essential role. On the one hand, radiation redistributes energy in the flow field, modifying the final temperature and acoustic modes of the combustor (Sengissen *et al.* 2007). On the other hand, heat transfer by conduction through the combustor walls determines the wall temperatures which are essential for combustion chambers design; e.g. in 2008 the CTR study of Kaess *et al.* (2008) showed that the response of a flame to acoustic excitations depended strongly on the flameholder temperature. Therefore, accounting for heat losses in LES of combustors is important. This can be done efficiently only if wall temperatures are well known, thus requiring a coupled computational approach. Performing LES for the flow and the chemistry while also accounting for radiation and conductive heat transfer is therefore one of the obvious promising paths for LES in the near future. It also belongs to a more general class of multi-physics problems studied for example at CTR in the PSAAP program. In the present work, LES of a reacting flow in a realistic combustion chamber (provided by Turbomeca) is coupled to the computation of radiation by combustion gases and to a heat conduction solver for the solid. A similar coupling methodology (limited to LES and heat transfer through walls) was first tested at CTR in 2008 by Duchaine *et al.* (2009) in a non-reacting case (blade cooling). The objective here is more ambitious and requires the coupling of three different solvers:

- A LES solver for flow and chemistry: here the LES solver of CERFACS (AVBP) is used.

<sup>†</sup> CERFACS, 42 Av. Coriolis, 31057 Toulouse, France

<sup>‡</sup> IMF Toulouse, INP de Toulouse and CNRS, 31400 Toulouse, France

- A radiation solver: a discrete ordinates method (DOM) solver developed by Ecole des Mines d'Albi and CERFACS (called PRISSMA) is coupled to AVBP.
- A heat conduction solver (AVTP), developed by CERFACS: this solver applied to the problem of heat conduction through the walls.

The objective is to evaluate the impact of heat conduction and radiation on the thermal behavior of the blade in the distributor downstream of the combustion chamber.

The characteristic time scales of each heat transfer mode are quite different: radiation has a negligible response time and radiative heat fluxes are established faster than any other phenomenon in the chamber. In the fluid, heat convection has a time scale  $\tau_F$ , which is controlled by the chamber size  $L$  and the bulk velocity  $U_b$  and is typically a few ms. Heat diffusion through the solid walls has a characteristic time scale of the order of a few seconds. Coupling the three solvers efficiently requires work at two levels. First, the stability of such coupled simulations remains difficult to control and a strategy to converge efficiently to the quasi steady state must be defined. Second, the parallel implementation of this three-code coupling is difficult: the issue is to split a given parallel machine in three parts (one for each solver) optimizing both the time between coupling points and the processor distribution between the three solvers to obtain the result in the shortest elapsed time. In the following, section 2 briefly presents the solvers. The configuration of the simulation is described in section 3. The results are then split into three parts: LES alone (section 4), LES with heat conduction (section 5) and LES with heat conduction and radiation (section 6).

## 2. Description of solvers and models

The different solvers used in this work have been extensively described before and are summarized here.

The LES is performed with the code AVBP, which solves the fully compressible Navier-Stokes equations together with the energy and chemical species conservation equations. It is based on a cell-vertex finite-volume formulation on unstructured meshes and uses up to third-order spatial and temporal discretization schemes. The sub-grid scale turbulence model used in the present work is the classical Smagorinsky model (Smagorinsky 1963), together with a wall law and turbulent Schmidt and Prandtl numbers of 0.6 for mixing. Turbulent combustion is described with the Thickened Flame model (Colin *et al.* 2000; L egier *et al.* 2000). Kerosene chemistry is simplified with a two-step kinetic scheme, validated for a wide range of initial pressure and temperature and for the whole range of equivalence ratio (Franzelli *et al.* 2010). Thermodynamic properties are tabulated so as to recover the correct temperature dependence.

The calculation of thermal diffusion in solids is performed with the code AVTP, solving the classical heat equation (Duchaine *et al.* 2009). AVTP also uses unstructured meshes and is advanced with a first-order explicit forward Euler scheme.

Finally the radiation solver, called PRISSMA, has been specifically designed for combustion applications (Joseph *et al.* 2005; Amaya *et al.* 2010). It uses DOM with different angular discretizations and spectral models. DOM allows to use the same kind of mesh as used in LES, which is a great advantage for the coupling. In the present work, the  $S_4$  quadrature (i.e. 24 directions) is used together with the tabulated FS-SNBcK spectral model (Poitou *et al.* 2009). This combination was shown by Poitou (2009) and Amaya (2010) to have sufficient accuracy with a reasonable computational cost.

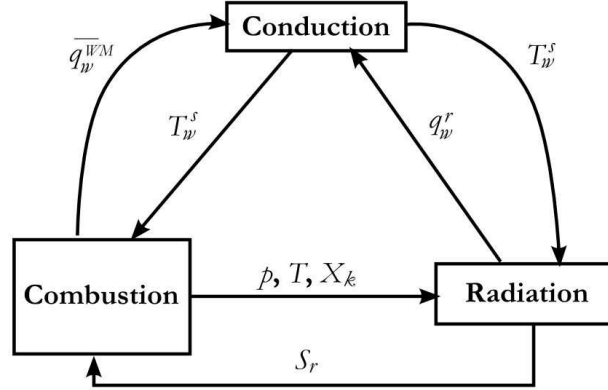


FIGURE 1. Interactions between combustion, radiation and heat conduction in solids.

The interactions between the three physical phenomena, i.e. combustion, radiation and heat transfer in the structure, are summarized in Fig. 1.

The coupling between AVBP and AVTP, as well as between PRISSMA and AVTP, is a surface coupling: data are exchanged at the boundaries of the flow/solid domain. To ensure stability (Giles 1997; Duchaine *et al.* 2009), AVBP and PRISSMA calculate and send to AVTP the convective and radiative heat flux, while AVTP sends back its surface temperature  $T_w^s$  which acts as a boundary condition for the flow, thus, influences the near-wall temperature in the fluid  $T_w^f$  as well as the wall radiative intensity. Note that  $T_w^f$  is not the temperature at the wall surface but of the first fluid node (this temperature differs from the wall temperature  $T_w^s$  because a law-of-the-wall formulation is used). The total heat flux to the wall writes:

$$q_w^s = q_w^{WM} + q_w^r = h_c^{WM}(T_w^f - T_w^s) + h^r(T_{ref}^r - T_w^s) \quad (2.1)$$

where  $q_w^r$  is the radiative heat flux and  $q_w^{WM}$  is the convective heat flux, calculated by the wall model in the fluid. To ensure convergence, the solvers do not exchange directly fluxes but reference temperatures in the fluid ( $T_w^f$  and  $T_{ref}^r$ ) and the heat transfer coefficients  $h_c^{WM}$  and  $h^r$  defined by:  $h_c^{WM} = q_w^{WM}/(T_w^f - T_w^s)$  and  $h^r = q_w^r/(T_{ref}^r - T_w^s)$ .

Through emission and absorption, radiation redistributes energy in the combustion chamber. This results in a volumic radiation source term  $\mathcal{S}_r$  added to the energy equation in AVBP. This source term being highly non-linear, it raises the question of the impact of the turbulent fluctuations of temperature and species mass fractions. Numerous studies have been devoted to this problem, known as the Turbulence-Radiation Interaction (TRI), mainly in the RANS context (Coelho 2007; Li & Modest 2007). It has been shown however that TRI is negligible in LES, where the sub-grid fluctuations are not high enough to modify radiation (Poitou 2009).

The coupling between PRISSMA and AVBP is volumic. AVBP sends its temperature, pressure and mass fraction fields to PRISSMA, while PRISSMA sends back the radiative source term.

The strong differences in time scales between the three physical phenomena requires a coupling strategy:

- The unsteady coupling of LES and heat transfer in solids is not synchronized in physical time: data exchange between the two codes is performed every  $\alpha_F \tau_F$  in the fluid and  $\alpha_s \tau_s$  in the solid, where  $\alpha_F$  and  $\alpha_s$  are the coupling synchronization constants. Each

---



---

|         | AVBP | AVTP | PRISSMA | CPU <sub>0.5</sub> |
|---------|------|------|---------|--------------------|
| Case AA | 230  | 24   | -       | 1 hr               |
| Case MP | 105  | 12   | 48      | 3 hr               |

---



---

TABLE 1. Processors distribution and CPU time. The quantity CPU<sub>0.5</sub> is the CPU time needed to compute 0.5 ms of physical time.

---

code has a different time step thus coupling is performed at different physical times. It has been shown by Duchaine *et al.* (2009) that using the same low value  $\alpha = \alpha_F = \alpha_s$  leads to a fast convergence to a steady state. In the asynchronous coupling strategy only the final equilibrium temperature field in the solid is kept, the intermediate states having no physical meaning.

- The radiation source term must be updated at time intervals corresponding to the characteristic time scale of the temperature and mass fractions, i.e.  $\tau_F$ . However, because AVBP is an explicit, fully compressible code, it runs with an acoustic time step  $\Delta t = CFL\Delta x/c$  where  $CFL$  is the Courant-Friedrich-Levy stability number,  $\Delta x$  is the mesh size and  $c$  is the speed of sound. Typically  $\tau_F \approx 100\Delta t$ , which means that the radiation source term can be updated every  $\approx 100$  iterations of LES (Leacanu 2005; Wang 2005).

All three solvers used here are efficiently parallelized; they use subdomain decomposition, and in the case of PRISSMA, the calculation is also parallelized using a spectral and angular discretization. However the three solvers have very different restitution times. AVTP is very fast (0.96 s/iteration/processor), as it involves a simple equation for only one variable, whereas PRISSMA is very long (3000 s/iteration/processor), mainly owing to the spectral complexity and the non-local character of the integration (optical paths go through the whole domain). AVBP is in between, with 95.2 s/iteration/processor, but requires many iterations. Efficient coupled simulations require an optimal load balancing, where resources allocation for each solver allows the synchronization of data exchanges (Amaya 2010). The management of data exchange and resources allocation is performed with a dedicated software (PALM) that allows for setting up and monitoring coupled simulations (Buis *et al.* 2005). Table 1 gives the processors distribution as well as CPU times for the different solvers in the two AVBP-AVTP (AA) and AVBP-AVTP-PRISSMA (MP) coupled simulations. Note that AVBP and AVTP run on half processors in the MP simulation compared with the AA simulation. Because PRISSMA reaches a speedup limit at 48 processors, load balancing and synchronization imply a limitation of processors on the two other codes.

### 3. Configuration

The configuration is a sector of a helicopter combustion chamber of Turbomeca (Fig. 2), including the secondary air flow (A) and the high pressure distributor containing one blade of the downstream stator (D) which redirects the flow in an azimuthal motion. The flame tube (C) is curved for compactness, and fed with air through two contra-rotating swirlers and gaseous kerosene at the center (B). Chamber cooling is achieved by cold air films along the walls. The main thermal problem here is linked to the blade,

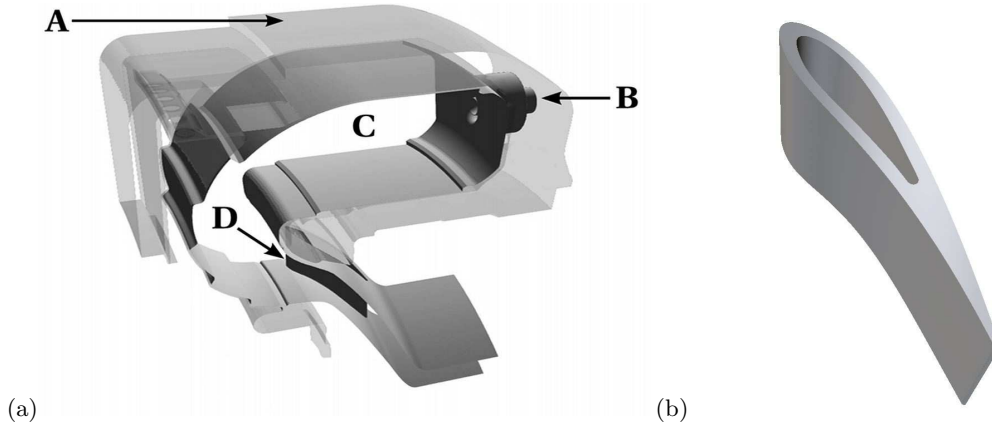


FIGURE 2. View of the configuration geometry (a) and detail of the blade (b).

which does not hold the high temperatures produced by the flame in the combustor. In order to decrease their temperature, the burnt gases are therefore mixed with cold air in the dilution zone of the combustion chamber. The challenge is to reach a homogeneous mixture at the chamber exit and guarantee the absence of hot spots that could damage the blade.

The blade geometry is also detailed in Fig. 2. It is cooled with an internal cold flow, represented in the present simulation with a fixed convective heat transfer coefficient. Note that in the true geometry additional cooling devices are also present, in particular at the trailing edge of the blade. These systems were not included here for simplicity.

The LES mesh is built with  $11.9 \cdot 10^6$  tetrahedra. It involves the secondary air flow, as well as all cooling films and primary and dilution jets. To describe the flame with sufficient accuracy, the mesh is refined in the primary zone where the flame stabilizes in a conical shape. For PRISSMA, only the combustion chamber is meshed with  $2.6 \cdot 10^6$  cells.

The calculated operating point corresponds to full thrust. An algebraic adiabatic law of the wall is used for all walls of the geometry, including the blade in the uncoupled AVBP simulation. The Lax-Wendroff scheme was used for all AVBP calculations. In the coupled simulations, heat transfer to the walls is calculated only for the blade, on a mesh made of  $10^6$  tetrahedra. The solid has a conductivity  $\lambda = 24$  [ $\text{WK}^{-1}\text{m}^{-1}$ ], a heat capacity  $C = 600$  [ $\text{Jm}^{-3}\text{K}^{-1}$ ], a density  $\rho = 8110$  [ $\text{kg}\cdot\text{m}^{-3}$ ] and a diffusivity  $a = 4.39 \times 10^{-6}$  [ $\text{m}^2\text{s}^{-1}$ ].

Radiation is computed considering only  $\text{H}_2\text{O}$ ,  $\text{CO}_2$  and  $\text{CO}$  as absorbing, and a constant wall emissivity of 0.95. Radiation is known to be very sensitive to the wall temperature, which makes the coupling with heat transfer in solids mandatory in confined flows. However in the present simulation, heat transfer is computed only in the blade, and the temperature of the chamber walls is prescribed from measurements.

#### 4. Turbulent reacting flow: uncoupled LES results

Figure 3 (left) shows the mean axial velocity, non-dimensionalized by the injection velocity, in the median plane for an uncoupled LES, where the main features of a swirled flow are recognized: a central recirculation zone (visualized with a zero-axial velocity contour) extends from the injector nozzle to approximately half the primary zone. Owing

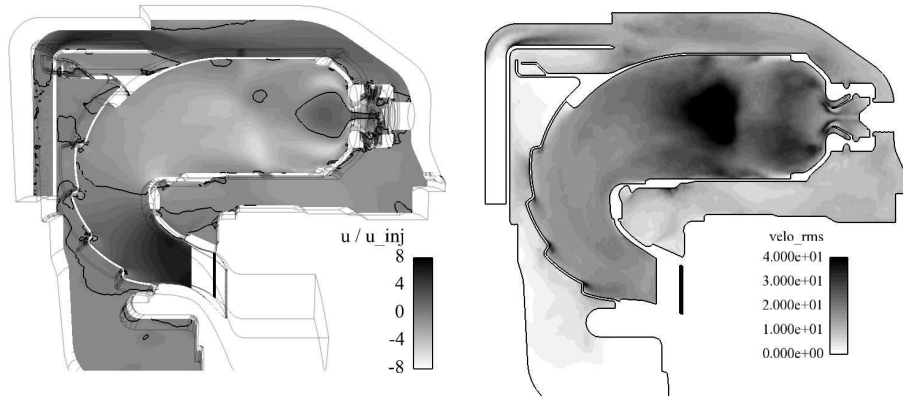


FIGURE 3. Mean axial velocity, non-dimensionalized by the injection velocity with an isocontour line at zero (left) and rms velocity (right) in the median plane. Uncoupled simulation (AVBP only).

to the curved geometry, the flow is not symmetric. After changing direction, it is strongly accelerated in the distributor. The rms axial velocity field (Fig. 3 right) indicates zones of high turbulence: close to the injection in high shear zones and behind the central recirculation zone, where the hot gas mix with the primary air jets.

Figure 4 displays the mean temperature, non-dimensionalized by the injection temperature  $T_{inj}$ , and the products mass fractions fields in the median plane. The hot primary zone reaches a maximum temperature of  $\approx 4T_{inj}$ , around the conical flame. The flame is asymmetric and the hot zone is more extended on the internal side. The hot gases are cooled down abruptly by the cold air jets, down to a temperature around  $2T_{inj}$ . The temperature of the burnt gases gradually decreases downstream through the action of the cooling films along the chamber walls, reaching a value around  $1.5T_{inj}$  near the blade. Although high turbulence levels in the dilution zone (Fig. 3 right) increases mixing, the temperature is not perfectly homogeneous at the chamber exit. Figure 4 also shows the distribution of the radiating species (combustion products), which are mostly located around the flame zone and strongly diluted downward. As a consequence, radiation emission by the gas will mainly originate from the flame zone.

### 5. Coupled LES/heat conduction simulations (AA case)

In a first step, only the two solvers, AVBP and AVTP, are coupled (AA case). The resulting temperature field in the blade shown in Fig. 5 is quite inhomogeneous, as a consequence of the heating by the hot gas and the cooling by the internal flow. A hot zone (HS1) is visible on the leading edge owing to the exposure of this surface to the hot flow. Another hot spot can be observed at the trailing edge (HS2), at an even higher temperature. In this zone the thinness of the solid limits heat conduction and leads to heat accumulation. Note also the temperature difference between the top and bottom of the blade, the result of cooling films in the chamber (see Fig. 5).

Fig. 6 gives the time-averaged non-dimensional temperature of the solid  $T_w^s/T_{inj}$ , the non-dimensional near-wall temperature of the fluid  $T_w^f/T_{inj}$  and the convective heat flux along a blade contour in the bottom, median and top cutting planes (contour points are shown in the bottom right image of Fig. 6). The mean flow impacts the blade almost

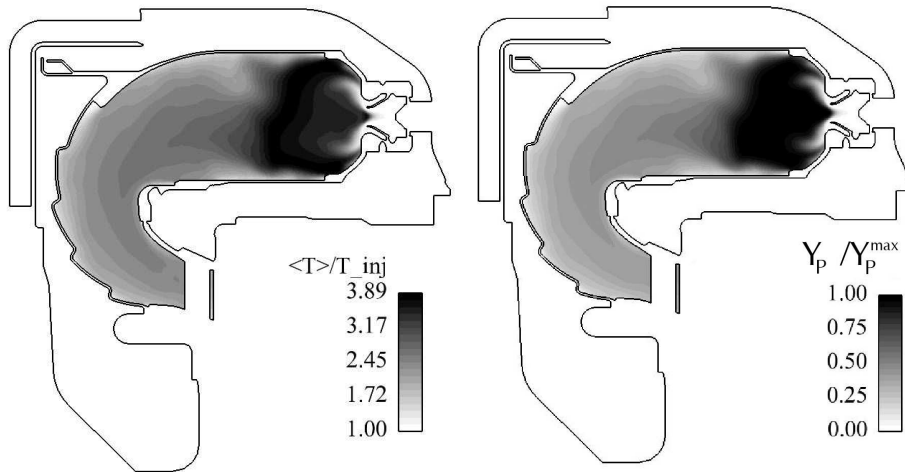


FIGURE 4. Mean temperature (non-dimensionalized by the injection temperature) (left) and products mass fractions  $Y_P = Y_{H_2O} + Y_{CO} + Y_{CO_2}$  (right) in the median plane. Uncoupled simulation (AVBP only).

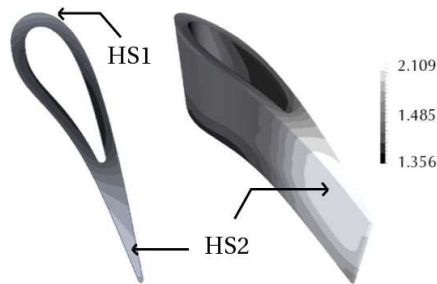


FIGURE 5. Blade temperature field in the mid-plane (non-dimensionalized by the injection temperature) (left) and on the surface (right). AA case.

horizontally relative to the image shown in Fig. 6: the stagnation point is situated around the point 22. The coupled AVBP-AVTP simulation (AA case, solid line in Fig. 6) introduces negative heat fluxes in the pressure side and leading edge of the blade and positive values on the trailing edge of the suction side. Between points 1 and  $\approx 15$ , the gas is hot and the blade surface temperature decreases because of the internal cooling, which leads to an increasing negative flux in the fluid. When approaching the leading edge (point 25), the blade temperature increases again and the flux, still negative, decreases in magnitude. Continuing along the suction side of the blade, the flux gradually decreases in magnitude as the gas temperature decreases, then changes sign and increases again as the blade temperature increases. Finally at the trailing edge on the suction side, the positive flux starts to decrease following the gas temperature increase. The impact of the AVBP-AVTP coupling on the fluid temperature is close to zero in the top and median plane but leads to a quite significant temperature decrease in the bottom plane compared with the uncoupled simulation (dashed line in Fig. 6). This may be due to the different thermal properties of the mixture in this zone, where cold films mix with hot gas.

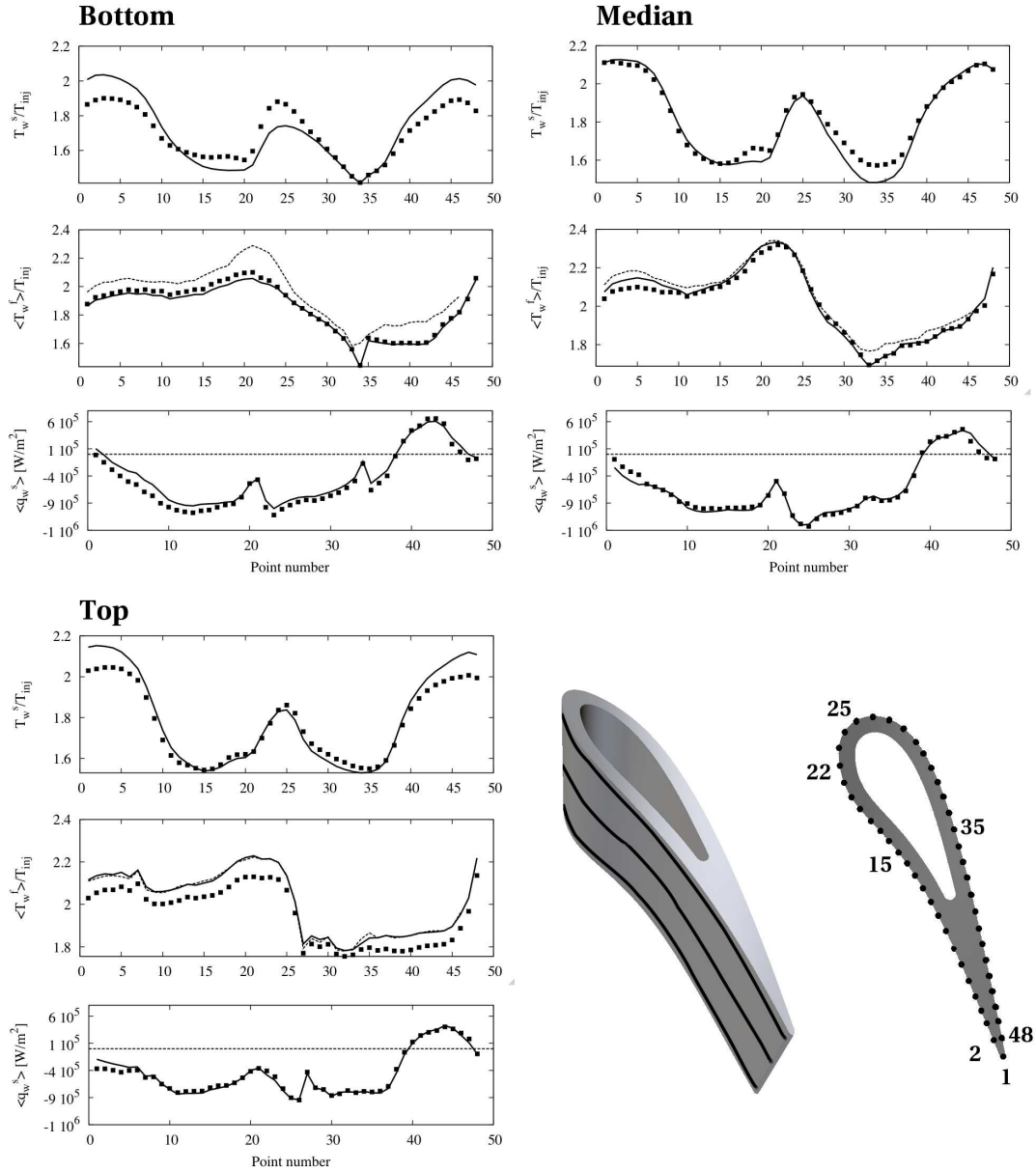


FIGURE 6. Profiles of adimensional temperature on the solid surface ( $T_w^s/T_{inj}$ ), in the near-wall fluid ( $T_w^f/T_{inj}$ ) and convective heat flux ( $q_w$ ) along the blade contour shown in the bottom right, for the top, median and bottom cutting planes. Dashed lines: AVBP alone. Thick lines: Coupled AVBP-AVTP simulation (AA case). Symbols: Coupled AVBP-AVTP-PRISSMA simulation (MP case).

## 6. Coupled LES, heat conduction and radiation simulation (MP case)

The three solvers are now coupled. Figure 7 shows the mean field of radiative source term (non-dimensionalized by  $Sr_{inj} = \sigma T_{inj}^4$  where  $\sigma$  is the Stefan-Boltzmann constant). It is clearly correlated to a zone where hot combustion products are located, particularly

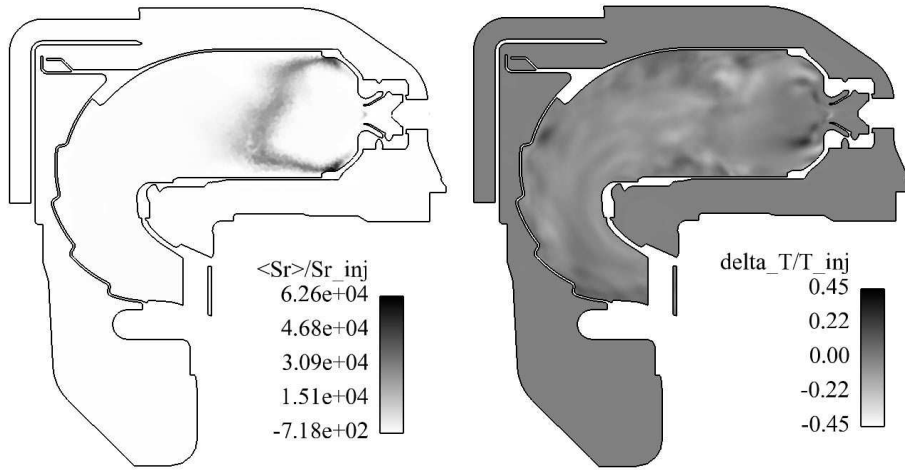


FIGURE 7. Left: Radiation source term in the median plane of the combustion chamber (non-dimensionalized by  $Sr_{inj} = \sigma T_{inj}^4$ ). Right: Mean non-dimensional temperature difference between the simulations with and without radiation in the median plane of the combustion chamber.

at the end of the primary zone where CO is formed. The radiative source term take negative values where the hot gases mix with cooling air. There is no direct effect of radiation on the blade, as there is no direct line of sight between the blade and the flame. However one may expect an indirect effect, through the modification of the flow temperature distribution. This is illustrated on Fig. 7(right), showing the mean non-dimensional temperature difference between the simulations with and without radiation in the median plane of the combustion chamber; hotter gases appear along the wall, whereas gases are cooled down in the center of the chamber.

Compared with the mean energy in the combustor, the mean radiative source term is small. It is approximately 4.8% of the combustion heat release, and leads to a temperature deviation of the same order (Fig. 8). This is usual for such small flames as energy emission or absorption cumulates along optical paths and strongly depend on the volume of hot gases. However a deviation of the gas temperature of 4.8% is an important difference in the context of blade cooling, suggesting that radiation must be calculated.

Finally Fig. 6 shows the non-dimensional blade temperature, the non-dimensional near-wall fluid temperature around the blade and the convective heat flux obtained when radiation is included (symbols). In the three planes the impact of radiation on the convective heat flux is negligible, but fluid temperatures  $T_w^f$  are modified. Differences also appear on the solid temperature  $T_w^s$ , as the blade surface receives a radiative flux (mostly at the leading edge) and emits radiation (mostly at the trailing edge).

## 7. Conclusions

Multi-physics simulations, including LES of turbulent reacting flow, heat conduction in solids, and radiative heat transfer, have been performed in a helicopter gas turbine. These coupled simulations allow for the study of the thermal behavior of the system taking into account the three heat transfer modes. In particular the problem of turbine blade cooling is critical for the design of the engine and requires a prediction of the temperature distribution with high precision: an error bar of 10K is the current objective

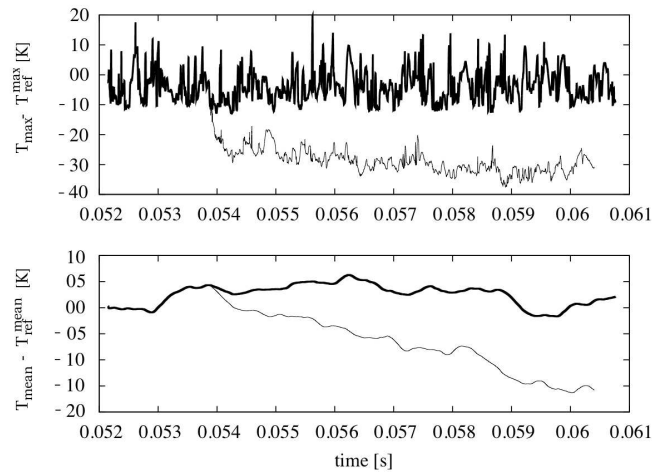


FIGURE 8. Time evolution of the maximum (top) and mean temperature (bottom) in the chamber relative to the arbitrary reference temperatures  $T_{ref}^{max}$  and  $T_{ref}^{mean}$ , for the simulations without radiation (thick line) and with radiation (thin line).

(an error of 25K can induce a reduction of 50% in the lifetime of the blade). The results show that, in the present configuration, both heat conduction in the solid and radiation have a non negligible impact on the fluid and the blade temperature.

The authors acknowledge the support of CINES (GENCI, France) for the computing resources (grant 2010-c2010026401) and Turbomeca for the case definition. We also thank Florent Duchaine (IMFT), Damien Poitou (CERFACS), and Thomas Lederlin (Turbomeca) for their support and helpful discussions.

#### REFERENCES

- AMAYA, J. 2010 Unsteady coupled convection, conduction and radiation simulations on parallel architectures for combustion applications. PhD thesis, INP Toulouse.
- AMAYA, J., CABRIT, O., POITOU, D., CUENOT, B. & EL HAFI, M. 2010 Unsteady coupling of Navier-Stokes and radiative heat transfer solvers applied to an anisothermal multicomponent turbulent channel flow. *J. Quant. Spec. Rad. Transf.* **111** (2), 295–301.
- BUIS, S., PIACENTINI, A. & DÉCLAT, D. 2005 PALM: A Computational Framework for assembling High Performance Computing Applications. *Concurrency. Comput.* **18** (2), 231–245.
- COELHO, P.J. 2007 Numerical simulation of the interaction between turbulence and radiation in reactive flows. *Prog. Energy Comb. Sci.* **33**, 311–383.
- COLIN, O., DUCROS, F., VEYNANTE, D. & POINSOT, T. 2000 A thickened flame model for large eddy simulations of turbulent premixed combustion. *Phys. Fluids* **12** (7), 1843–1863.
- DUCHAINE, F., CORPRON, A., PONS, L., MOUREAU, V., NICOD, F. & POINSOT, T. 2009 Development and assessment of a coupled strategy for conjugate heat transfer with Large Eddy Simulation. application to a cooled turbine blade. *Int. J. Heat Fluid Flow* **30** (6), Pages 1129–1141.

- FRANZELLI, B., RIBER, E., SANJOSÉ, M. & POINSOT, T. 2010 A two-step chemical scheme for large eddy simulation of kerosene-air flames. *Combust. Flame* **157** (7), 1364–1373.
- GILES, M.B. 1997 Stability analysis of numerical interface conditions in fluid-structure thermal analysis. *Int. J. Numer. Meth. Fluids* **25**, 421–436.
- JOSEPH, D., EL HAFI, M., FOURNIER, R. & CUENOT, B. 2005 Comparison of three spatial differencing schemes in discrete ordinates method using three-dimensional unstructured meshes. *Int. J. Therm. Sci.* **44** (9), 851–864.
- KAESS, R., POLIFKE, W., POINSOT, T., NOIRAY, N., DUROX, D., SCHULLER, T. & CANDEL, S. 2008 Cfd-based mapping of the thermo-acoustic stability of a laminar premix burner. In *Proc. of the Summer Program*, pp. 289–302. Center for Turbulence Research, NASA AMES, Stanford University, USA.
- LACAZE, G., CUENOT, B., POINSOT, T. J. & OSCHWALD, M. 2009 Large eddy simulation of laser ignition and compressible reacting flow in a rocket-like configuration. *Combust. Flame* **156** (6), 1166–1180.
- LEACANU, M. 2005 Couplage multi-physique combustion turbulent - rayonnement - cinétique chimique. PhD thesis, Ecole centrale Paris.
- LÉGIER, J.-PH., POINSOT, T. & VEYNANTE, D. 2000 Dynamically thickened flame LES model for premixed and non-premixed turbulent combustion. In *Proc. of the Summer Program*, pp. 157–168. Center for Turbulence Research, NASA Ames/Stanford Univ.
- LI, G. & MODEST, M.F. 2007 Numerical simulation of turbulence radiation interaction in turbulent reacting fluxes. *Modelling and Simulation of Heat Transfer* pp. 77–109.
- MAHESH, K., CONSTANTINESCU, G., APTE, S., IACCARINO, G., HAM, F. & MOIN, P. 2006 Large eddy simulation of reacting turbulent flows in complex geometries. In *ASME J. Appl. Mech.*, vol. 73, pp. 374–381.
- MOIN, P. & APTE, S. V. 2006 Large-eddy simulation of realistic gas turbine combustors. *Am. Inst. Aeronaut. Astronaut. J.* **44** (4), 698–708.
- POITOU, D. 2009 Radiation modelling in large eddy simulation of turbulent combustion. PhD thesis, INP Toulouse.
- POITOU, D., AMAYA, J., BHUSHAN SINGH, C., JOSEPH, D., ELHAFI, M. & CUENOT, B. 2009 Validity limits for the global model FS-SNBcK for combustion applications. In *Eurotherm83 — Computational Thermal Radiation in Participating Media III*. Lisbon, Portugal.
- SCHMITT, P., POINSOT, T., SCHUERMANS, B. & GEIGLE, K. P. 2007 Large-eddy simulation and experimental study of heat transfer, nitric oxide emissions and combustion instability in a swirled turbulent high-pressure burner. *J. Fluid Mech.* **570**, 17–46.
- SENGISSEN, A., KAMPEN, J. F. VAN, HULS, R., STOFFELS, G., KOK, J. B. W. & POINSOT, T. 2007 Les and experimental studies of cold and reacting flows in a swirled partially premixed burner with and without fuel modulation. *Combust. Flame* **150**, 40–53.
- SMAGORINSKY, J. 1963 General circulation experiments with the primitive equations: 1. the basic experiment. *Mon. Weather Rev.* **91**, 99–164.
- WANG, Y. 2005 Direct numerical simulation of non-premixed combustion with soot and thermal radiation. PhD thesis, University of Maryland.